AGU ADVANCING EARTH AND SPACE SCIENCE

Geophysical Research Letters

RESEARCH LETTER
10.1029/2020GL090726

Lower-Hybrid-Drift Vortices in the Electron-Scale Magnetic Reconnection Layer

J. Ng[1,2], L.-J. Chen[2], A. Le[3], A. Stanier[3], S. Wang[1,2], and N. Bessho[1,2]

[1]Department of Astronomy, University of Maryland, College Park, MD, USA, [2]NASA Goddard Space Flight Center, Greenbelt, MD, USA, [3]Los Alamos National Laboratory, Los Alamos, NM, USA

Key Points:
- The lower-hybrid-drift instability (LHDI) is excited immediately downstream of the electron jet reversal in guide field reconnection
- The LHDI propagates downstream as alternating vortices in channels of enhanced electron outflow
- The LHDI causes kinking of the electron outflow, small patches of increased current, and local perturbations to the guide field

Correspondence to:
J. Ng,
jonng@umd.edu

Citation:
Ng, J., Chen, L.-J., Le, A., Stanier, A., Wang, S., & Bessho, N. (2020). Lower-hybrid-drift vortices in the electron-scale magnetic reconnection layer. *Geophysical Research Letters*, *47*, e2020GL090726. https://doi.org/10.1029/2020GL090726

Received 11 SEP 2020
Accepted 8 NOV 2020
Accepted article online 10 NOV 2020

Abstract Lower-hybrid-drift waves driving vortical flows have recently been discovered in the electron current layer during magnetic reconnection in the terrestrial magnetotail. Yet, spacecraft measurements cannot address how pervasive the waves are. We perform three-dimensional particle-in-cell simulations of guide field reconnection to demonstrate that electron vortices driven by the lower-hybrid-drift instability (LHDI) are excited immediately downstream from the electron jet reversal in 3-D channels of enhanced electron outflow. The resulting fluctuations generate a series of alternating vortices, producing magnetic field perturbations opposing and enhancing the local guide field and causing kinking of the enhanced electron outflow and patches of increased current. Our results demonstrate for the first time that LHDI exists in the electron current layer and enhanced outflow channels, providing a conceptual breakthrough on the LHDI in reconnection.

Plain Language Summary Lower-hybrid-drift waves have been discovered in the electron-scale reconnection layer by the Magnetospheric Multiscale (MMS) mission in the Earth's magnetotail. These waves drive vortical electron flows and modify the magnetic field along the reconnection current. We perform fully kinetic simulations which demonstrate how these waves can be generated and their effects on the electron dynamics and magnetic fields in the reconnection region.

1. Introduction

Magnetic reconnection is a process in which the magnetic field lines in a plasma change their topology by breaking and reconnecting (Dungey, 1953), with the conversion of stored magnetic energy to kinetic energy of accelerated particles. Reconnection plays an important role in many laboratory and space plasma processes including sawtooth crashes in tokamaks, solar flares, magnetic substorms in the Earth's magnetosphere, and coronal mass ejections (Bhattacharjee et al., 2001; Phan et al., 2000; Vasyliunas, 1975; von Goeler et al., 1974; Yamada et al., 2010).

The lower-hybrid-drift instability (LHDI) is an instability excited in inhomogeneous plasmas by the diamagnetic current drifting across the magnetic field (Davidson et al., 1977; Hirose & Alexeff, 1972; Huba & Wu, 1976; Krall & Liewer, 1971). Earlier work on the LHDI has shown that can be important during reconnection by causing turbulence and enhancing transport at the separatrix (Le et al., 2017; Price et al., 2016). Recent observations by the Magnetospheric Multiscale (MMS) mission in the Earth's magnetotail have shown the presence of electron-gyroradius scale ($k_\perp \rho_e \sim 1$, where $k_\perp$ is the wavenumber perpendicular to the magnetic field and ρ_e is the electron gyroradius) lower-hybrid fluctuations propagating in the reconnection layer during guide field reconnection (Chen et al., 2019). These fluctuations were found to cause electron vortical flows and nongyrotropic heating (Chen et al., 2020).

The MMS discovery inspires new questions and possibilities about how the LHDI may impact reconnection physics. First, we distinguish the MMS-discovered LHDI from previous simulation and observational studies of the LHDI related to reconnection. Typically, the short-wavelength LHDI with $k_\perp \rho_e \sim 1$ is observed at the upstream edge of the current sheet (Carter et al., 2001), the downstream jet front where the outflow interacts with the ambient plasma (Divin et al., 2015; Lapenta et al., 2018; Nakamura et al., 2019) and is stabilized at the center of the current layer (Carter et al., 2002; Daughton, 2003), while only the longer wavelength electromagnetic LHDI with $k\sqrt{\rho_e \rho_i} \sim 1$ is found at the centre of the current sheet. The LHDI has been shown to cause electromagnetic fluctuations in simulations (Daughton, 2003) and laboratory experiments

(Ji et al., 2004), which may contribute to anomalous resistivity and viscosity (Le et al., 2017; Price et al., 2016; Roytershteyn et al., 2012).

In order to understand how the lower-hybrid structures are generated in the electron-scale reconnection layer and assess how pervasive they are, we perform fully kinetic particle-in-cell simulations of guide field reconnection. We demonstrate that the three-dimensional structure of the current sheet causes regions of enhanced outflow velocity and density gradient immediately downstream of the electron jet reversal region and these regions are unstable to the LHDI. The LHDI is driven by the in-plane outflow currents rather than the out-of-plane current sheet. The excited lower-hybrid fluctuations modify the electron flow, leading to perpendicular electron-scale vortices embedded in the outflow, the kinking of the ouflow, small patches of increased current, and the enhancement and reduction of the guide magnetic field. Our results provide a mechanism to account for the lower-hybrid fluctuations observed in the electron-scale reconnection region by MMS (Chen et al., 2020).

2. Simulation Setup

We perform two- and three-dimensional kinetic simulations using the particle-in-cell code VPIC (Bowers, Albright, Bergen, et al., 2008; Bowers, Albright, Yin, et al., 2008). The initial setup is a force-free current sheet with uniform density n_0. Once reconnection saturates, the features of the current sheet are relatively insensitive to the initial conditions and depend mainly on the upstream plasma parameters. Although the current sheet is initially force-free, density gradients develop as the system evolves. The initial magnetic field components are given by

$$\begin{aligned} B_x(z) &= B_0 \tanh\left(\frac{z}{L}\right) \\ B_y(z) &= -\sqrt{B_0^2 - B_x(z)^2 + B_g^2} \\ B_z(z) &= 0. \end{aligned} \tag{1}$$

The physical parameters used in this simulation are $m_i/m_e = 300$, $\omega_{pe}/\omega_{ce} = 1$, $T_i/T_e = 5$, $B_g/B_0 = 0.3$, and $\beta_e = 0.1$. Here m_i, m_e, T_i, and T_e are the ion and electron masses and temperatures respectively, ω_{pe} the electron plasma frequency, ω_{ce} the electron cyclotron frequency, and β_e the ratio of electron pressure to magnetic pressure. We set the initial width of the current sheet $L = d_i$, where d_i is the ion inertial length. The simulation domain is $L_x \times L_y \times L_z = 20d_i \times 20d_i \times 20d_i$ with 1792 cells in each direction and is initialized with 150 particles per species per cell, giving a total of roughly 1.7×10^{12} particles in the simulation. The simulation uses open boundary conditions (Daughton et al., 2006) in the x and z directions, and periodic boundary conditions in the y direction. The initial current is carried by the electrons and is given by Ampère's law. Reconnection is initiated by a small perturbation in the magnetic field which causes an X-line to develop at the centre of the domain in a manner similar to (Le et al., 2019), which focused on the study of electron-anisotropy-driven instabilities. We also perform a 2-D simulation in the x-z plane with the same parameters for comparison. Unless otherwise specified, we use simulation units with $d_e = 1, c = 1$, and $\omega_{pe} = 1$. The mass ratio of 300 provides a sufficient separation of scales to see the LHDI physics (Daughton, 2003).

3. Results

The data used in this paper are from the time slices $t\Omega_{ci} = 23.75$ and 24.25, after the onset of reconnection but before the formation of the anisotropy-supported extended current layer in the exhaust (Le et al., 2013, 2019). These slices are chosen because the lower-hybrid structures can be seen clearly. The LHDI activity persists at later stages, but there is also growth of electron-scale anisotropy-driven instabilities (discussed in Le et al., 2019), which makes it more difficult to analyze the LHDI alone. Clear LHDI signatures are visible up to $t\Omega_{ci} = 36$.

The overall structure of the reconnection region is shown in Figure 1a, a volume rendering of the current density j_y in a subset of the domain. As is typical for a three-dimensional system, regions of strong density gradient around the current sheet and separatrix are unstable to electrostatic and electromagnetic lower-hybrid drift instabilities (Lapenta et al., 2003; Le et al., 2017, 2019; Price et al., 2016; Roytershteyn et al., 2012). There are larger-scale fluctuations of the current sheet and exhaust with $k_y\sqrt{\rho_e\rho_i} \approx 0.5$, which

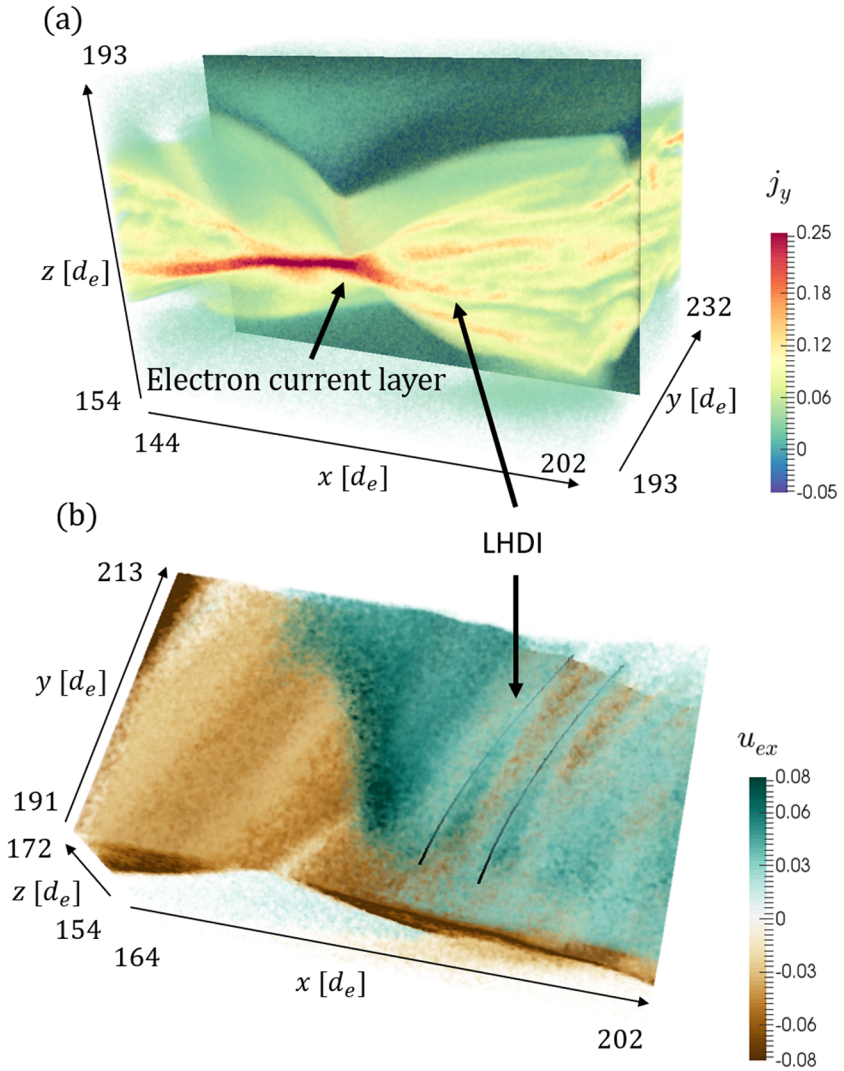

Figure 1. Three-dimensional view of the electron current layer and jet reversal showing the LHDI-unstable region. (a) Volume rendering of the current density j_y at $t\Omega_{ci} = 24.25$ in the 3-D simulation. An x-z plane is shown for visual reference. This shows a subset of the entire domain, which is $(346d_e)^3$. (b) Volume rendering of u_{ex} showing the unstable region in the bottom-right quadrant. The black lines approximately parallel to the u_{ex} fluctuations are the magnetic field lines showing that $\vec{k} \cdot \vec{B} \approx 0$.

is likely to be caused by the electromagnetic LHDI (Le et al., 2017, 2019). In this paper we focus on the localized region immediately downstream of the electron jet reversal which is unstable to the LHDI as shown in Figure 1b. This shows a volume rendering of the electron velocity u_{ex} in the bottom-right quadrant which provides the perpendicular current driving the instability. The fluctuations in u_{ex} are signatures of the LHDI, as we will show later on in the paper. The black lines are magnetic field lines in the unstable region and show that $\vec{k} \cdot \vec{B} \approx 0$, consistent with the characteristics of the LHDI. The structure of the LHDI can also be seen in Figure 1a, in which there are fluctuations of j_y which appear as patches of increased current.

This is not the only region which is unstable to the LHDI. Figure 2 shows the electron velocity components u_{ex} and u_{ez} in the x-y plane for the entire y extent of the simulation domain. The slice is approximately 1 d_e below the midplane and reveals multiple regions of enhanced u_{ex} on the right side of the plot. These regions are unstable to the LHDI, which can be seen in both the u_{ex} fluctuations and the u_{ez} reversals.

Figure 3 shows the structure and time evolution of the electron velocity fields u_{ex} and u_{ez} at the times $t\Omega_{ci} = 23.75$ and 24.25 in the region around $y = 200, z = 172.2$, $180 < x < 200$ (y and z are marked by the dashed lines in Figures 2 and 3). The lower-hybrid fluctuations we study can be found in the region where u_{ex}

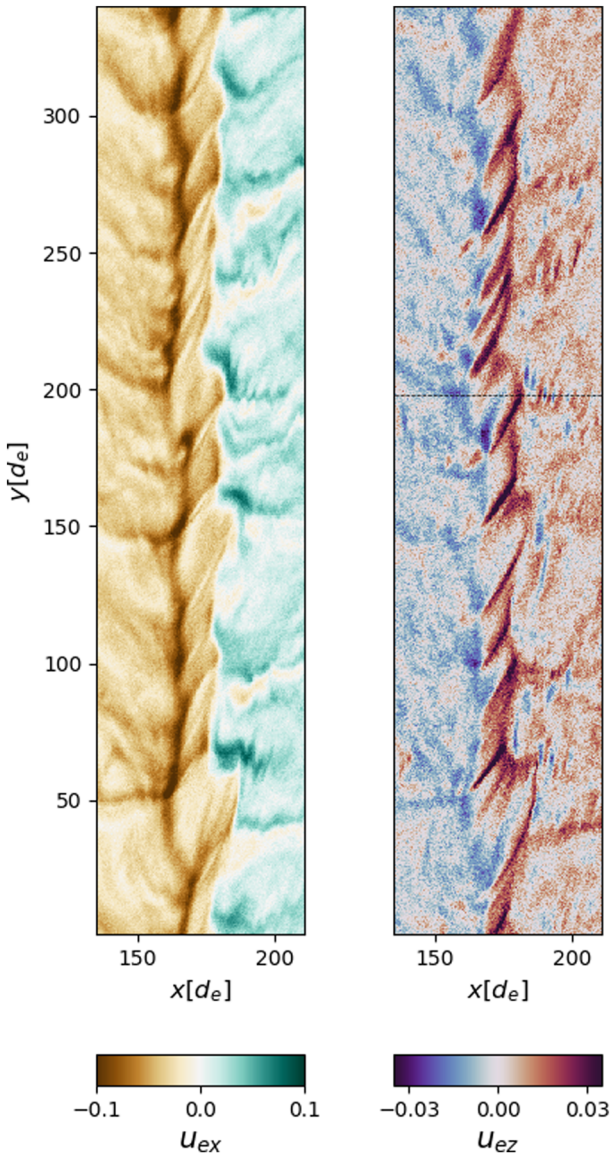

Figure 2. Two-dimensional slices showing the electron velocities (left) u_{ex} and (right) u_{ez} in the x-y plane at $z = 172.2$ (approximately 1 d_e below the midplane as shown by the dashed line in Figure 3). There are multiple channels with large u_{ex} (dark green) for $x \gtrsim 180$. These are unstable to the LHDI as shown by the kinking in u_{ex} and reversals in u_{ez}. We focus on the region marked by the dashed line, which shows the position of the x-z cuts in other figures.

is largest starting around $x = 182$ (close to the dotted lines in the u_{ex} plots) and are propagating in the outflow direction. The fluctuations extend in the y direction, as has been shown earlier in Figure 1b. There are fluctuations in both u_{ex} and u_{ez}, causing the kinking in the structure of u_{ex} and reversals in u_{ez} seen in Figure 3. These velocity perturbations correspond to E_z and E_x fluctuations respectively, as shown in Figure 4. There is also a local density gradient in z, consistent with the physical picture of the LHDI, and the ion x velocity is approximately 10× smaller in the unstable region. As such, we neglect u_{ix} in subsequent calculations. This behavior is consistent with the characteristics of the short-wavelength $k\rho_e \sim 1$ LHDI (Davidson et al., 1977).

Because of the presence of the guide field B_y, the E_x fluctuations of the LHDI cause the electrons to $\vec{E} \times \vec{B}$ drift in the z direction, as shown by the u_{ez} reversals. This causes the kinking in the structure of u_{ex} visible in the x-y and x-z planes of Figure 3. As is expected for the LHDI, for which the growth rate is fastest for waves perpendicular to the magnetic field, the fluctuating u_{ex} structures are approximately aligned with the field lines in Figure 1b, indicating perpendicular propagation. It should also be noted that the guide field B_y in this quadrant of the reconnection region is enhanced by the Hall magnetic field, so that $k_x \gg k_y$ for perpendicular

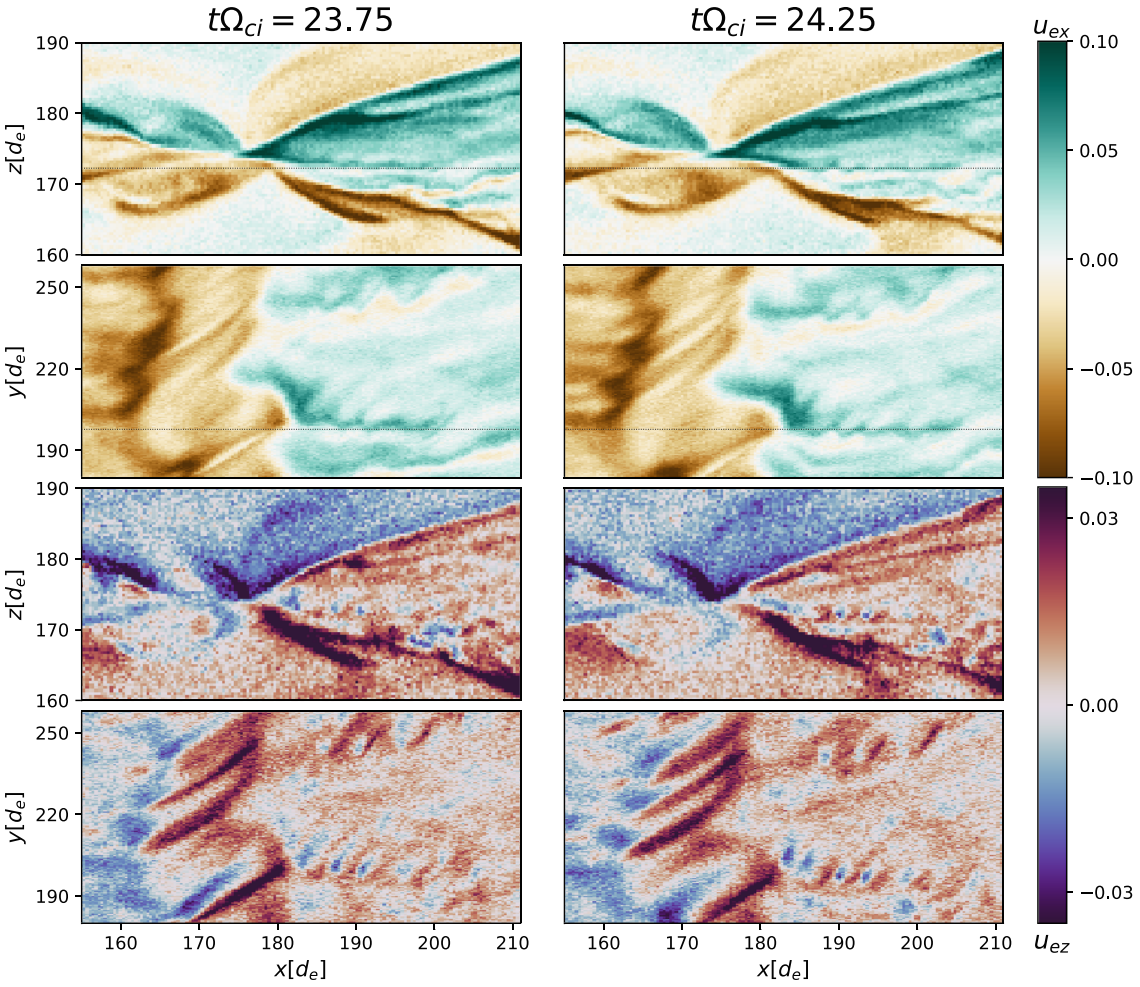

Figure 3. Slices in x-z and x-y taken from a subset of the 3-D domain around the region where the LHDI is observed from two time slices. The top four panels show u_{ex} and the bottom four panels show u_{ez}. The horizontal lines in the x-y plane show the position of the x-z slices, while the x-y slices are at $z = 172.2$. The LHDI occurs to the right of $x \approx 182$, $y \approx 200$, $z \approx 172$.

modes close to the B_x reversal. This is also true for fluctuations in the left outflow of the simulation, where the LHDI is observed in the top-left quadrant where u_{ex} is mostly perpendicular to the magnetic field.

In the slice shown in Figure 3, the LHDI is propagating approximately −14° from the x axis (i.e., in the positive x, negative y, z directions). The phase speed is $v_{ph} = 0.02$, less than half of the electron outflow velocity so that waves are propagating away from the X-line but are slower than the electron outflow. The wavelength is approximately $3.7d_e = 10\rho_e$ which corresponds to $k_\perp \rho_e \approx 0.63$. This gives a real frequency of $\omega \approx 0.039\omega_{pe} = 0.81\omega_{lh}$, where $\omega_{lh} = \omega_{pi}/\sqrt{1 + \omega_{pe}^2/\omega_{ce}^2}$ is the lower-hybrid frequency. We perform a linear analysis of the stability of the exhaust region to the LHDI (Davidson et al., 1977), including finite-beta and electromagnetic effects which are important in this regime. The parameters are taken from the region of large u_{ex} around $z = 172$, $185 < x < 195$. We use the following in the dispersion calculation: $n = 1.1$, $B = 0.73$, $\beta_e = 0.14$, $\beta_i = 1.13$, $u_\perp = 0.048$, $d(\ln n)/dz = 0.18$, $d(\ln B)/dz = -0.065$, $d(\ln T_e)/dz = -0.17$.

The dispersion relation reveals that the fastest growing mode has $k_\perp \rho_e \approx 0.6$, with frequency $\omega = 0.92\omega_{lh}$ and growth rate $\gamma = 0.24\omega_{lh}$. The magnitude of the fluctuating electric field is also consistent with the energy density after saturation $\mathcal{E} \sim nm_e V_d^2 / \left[4(1 + \omega_{pe}^2/\omega_{ce}^2)\right]$, where V_d is the relative perpendicular flow between electrons and ions (Davidson & Gladd, 1975). As mentioned earlier, the LHDI can also be generated at the separatrices, with comparable growth rates $\gamma \approx 0.1$–$0.3\omega_{lh}$ and a slightly longer wavelength of $5.5d_e$ for the fastest growing modes. There is also a larger k_y component as B_x increases away from the midplane. Aside from the local regions with strong $u_{e\perp x}$ which we discuss, the outflow region is stable to the LHDI.

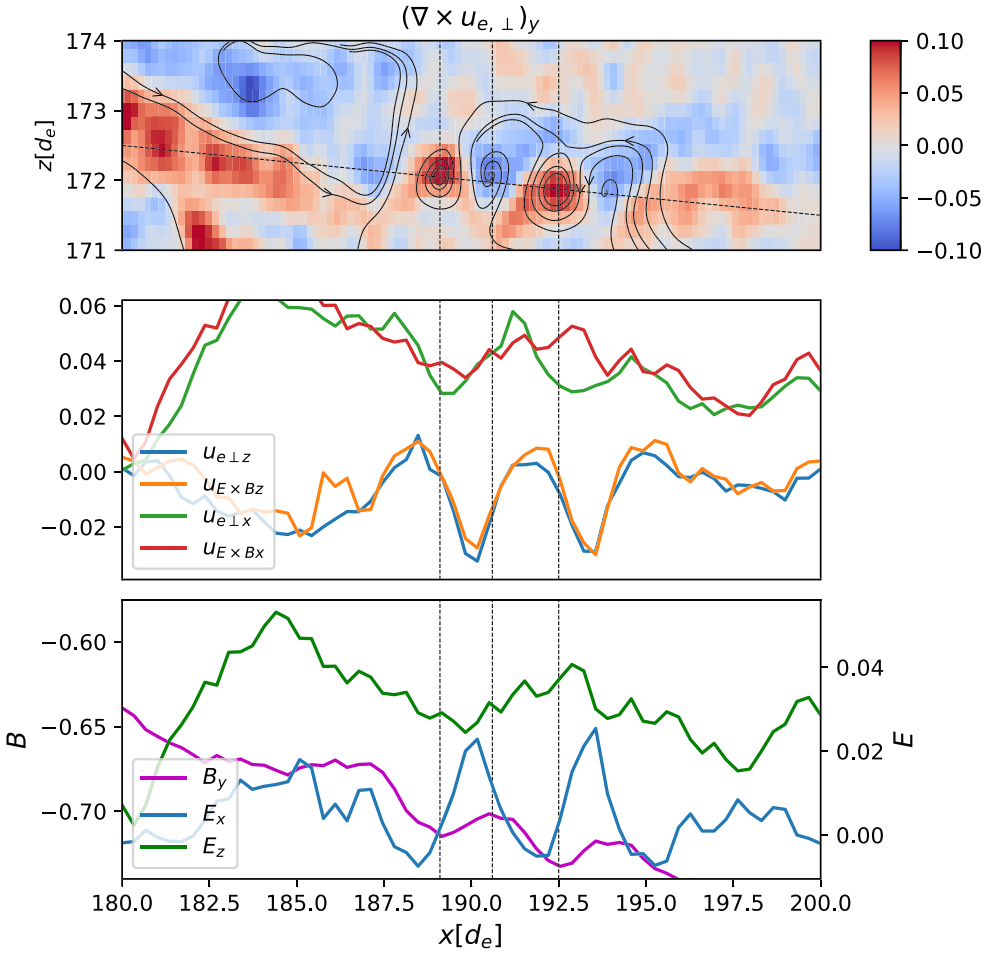

Figure 4. (top) Streamlines of perpendicular electron velocity in the background flow frame plotted over the y component of $\nabla \times \vec{u}_{e,\perp}$ at $t\Omega_{ci} = 24.25$. (middle) One-dimensional cuts along the diagonal dashed line through the lower-hybrid structures ($185 < x/d_e < 200$). Within this region, the $E \times B$ drift tracks the perpendicular electron velocity. (bottom) Electric and magnetic field fluctuations showing there is a strong electrostatic component E_x along the direction of propagation. Enhancement and reduction of the guide field B_y are consistent with the vortical electron flow.

Modifications to the perpendicular electron flow are further illustrated in the top panel of Figure 4, which shows the streamlines of the in-plane perpendicular velocity after subtraction of the mean velocity in the fluctuating region. The combination of the velocity perturbations from the LHDI and the region of enhanced flow, which creates a region of velocity shear, leads to the formation of alternating clockwise and counter-clockwise vortices with scales of 1–2 d_e in this frame, as seen in the alternating sign of the y component of $\nabla \times \vec{u}_{e,\perp}$, consistent with MMS observations (Chen et al., 2020).

The one-dimensional structure of the velocity and fluctuations at fixed y is shown in the middle panel of Figure 4. Here the in-plane electron perpendicular velocities along a 1-D cut passing through the vortices are shown. In the region where the LHDI is observed ($185 < x < 200$), both the bulk electron flow and the fluctuations are $\vec{E}\times\vec{B}$ driven as shown by the perpendicular velocity tracking the $\vec{E}\times\vec{B}$ drift. The corresponding electric fields are shown in the bottom panel, together with B_y fluctuations. Due to the modifications to the electron flow, which are perpendicular currents, the guide field is enhanced and reduced in the centre of the vortices (dashed lines in Figure 4). In the simulation the magnitude of these fluctuations $\Delta B/B < 0.05$, which is less than that observed by MMS (Chen et al., 2020), because of the lower saturation amplitude of the LHDI in the simulation due to the smaller outflow velocity.

The lower-hybrid fluctuations are not observed in the equivalent 2-D simulation we performed. As mentioned before, the fastest growing modes are expected to have a small but finite k_y based on the magnetic field in this region. This is not possible in the 2-D simulation with no y extent, and the LHDI becomes stabilized

away from perpendicular propagation (Gladd, 1976). Additionally, the outflow velocity in the 2-D simulation is smaller. This is likely due to the lack of modulation of the reconnection region as shown in Figures 1 and 3, which leads to regions where the outflow velocity and density gradient are larger in localized regions of the 3-D simulation. Using the dispersion relation with the parameters from the 2-D simulation, we find that similar locations in the 2-D simulation are stable to the lower-hybrid instabilities with $k_y = 0$. This may explain why the LHDI driven in the outflow direction is not seen in existing 2-D simulations though the propagation is mostly in the x-z plane.

The location and generation of the LHDI discussed here differs from what is expected in eigenmode studies (Daughton, 1999, 2003) and other simulations (Divin et al., 2015; Lapenta et al., 2018; Le et al., 2017; Nakamura et al., 2019; Price et al., 2016; Roytershteyn et al., 2012). Here the perpendicular current and density gradient associated with the generation of the LHDI are found in the electron outflow rather than the edge of the current sheet, the separatrix surface or where the jet interacts with the ambient downstream plasma, and the electron flow driving the instability is in the outflow direction rather than being part of the initial equilibrium causing the direction of propagation of the LHDI to be mostly in the x direction.

As mentioned earlier, the presence of the guide field is important for the LHDI discussed in this paper to be observed. The magnetic field is primarily in the y direction, and the guide field is enhanced by the Hall field in the quadrants where the LHDI is found. The electron outflow is magnetized and has a large perpendicular component which follows the local $E \times B$ drift, leading to the perpendicular current which is important for driving the LHDI.

4. Discussion

We now compare the vortices observed by MMS with those in our 3-D PIC simulation. In both cases, the LHDI occurs immediately downstream of the electron jet reversal and in the electron outflow. They have a strong electrostatic E_x component and have spatial scales comparable to the width of the electron current layer. What MMS captures is the LHDI within one electron jet channel, and does not allow the assessment of how pervasive the LHDI is. Even though the LHDI in the PIC simulation is not as intense as that observed by MMS, the simulation results show that the LHDI is unstable in multiple channels of enhanced electron outflow which provide a perpendicular current to the guide field, the dominant component of the magnetic field in the unstable regions.

To conclude, our results demonstrate for the first time the presence and dynamics of the LHDI in the electron current layer and channels of enhanced outflow, opening up new possibilities in 3-D reconnection research. In the three-dimensional simulation, we find that the LHDI occurs immediately downstream of the electron jet reversal in regions of strong electron outflow in the midplane of the reconnection layer, in contrast to the predictions of current sheet models in which the $k_\perp \rho_e \sim 1$ LHDI is only expected to develop at the edge of the current sheet, and only the longer wavelength variant of the LHDI can develop at the centre of the current sheet (Daughton, 2003). The LHDI we find propagates perpendicular to the local magnetic field, mainly in the outflow direction, modifying the out-of-plane current and electron flow patterns, and can be seen as perpendicular vortices embedded in the outflow. These perpendicular electron flows locally enhance or reduce the guide field. This mechanism may be responsible for the lower-hybrid fluctuations observed by MMS in the event discussed in (Chen et al., 2020), which caused vortical flows that modified the guide field.

Data Availability Statement

The data used in the figures are available online at (Ng et al., 2020). Full data are archived at NASA HECC.

Acknowledgments
This work was supported by DOE Grant DESC0016278, NSF Grant AGS-1619584, NASA Grant 80NSSC18K1369. A. L. was supported by NASA grant NNH17AE36I. Simulations were performed using NASA HECC resources.

References

Bhattacharjee, A., Ma, Z. W., & Wang, X. (2001). Recent developments in collisionless reconnection theory: Applications to laboratory and space plasmas. *Physics of Plasmas*, *8*(5), 1829–1839. https://doi.org/10.1063/1.1353803

Bowers, K. J., Albright, B. J., Bergen, B., Yin, L., Barker, K. J., & Kerbyson, D. J. (2008). 0.374 pflop/s trillion-particle kinetic modeling of laser plasma interaction on roadrunner. In *Proceedings of the 2008 ACM/IEEE Conference on Supercomputing* (pp. 63:1–63:11). SC '08. Piscataway, NJ, USA: IEEE Press.

Bowers, K. J., Albright, B. J., Yin, L., Bergen, B., & Kwan, T. J. T. (2008). Ultrahigh performance three-dimensional electromagnetic relativistic kinetic plasma simulation. *Physics of Plasmas*, *15*(5), 55703. https://doi.org/10.1063/1.2840133

Carter, T. A., Ji, H., Trintchouk, F., Yamada, M., & Kulsrud, R. M. (2001). Measurement of Lower-Hybrid drift turbulence in a reconnecting current sheet. *Physical Review Letters*, *88*, 15001. https://doi.org/10.1103/PhysRevLett.88.015001

Carter, T. A., Yamada, M., Ji, H., Kulsrud, R. M., & Trintchouk, F. (2002). Experimental study of lower-hybrid drift turbulence in a reconnecting current sheet. *Physics of Plasmas*, *9*(8), 3272–3288. https://doi.org/10.1063/1.1494433

Chen, L.-J., Wang, S., Le Contel, O., Rager, A., Hesse, M., Drake, J., et al. (2020). Lower-hybrid drift waves driving electron nongyrotropic heating and vortical flows in a magnetic reconnection layer. *Physical Review Letters*, *125*. https://doi.org/10.1103/PhysRevLett.125.025103

Chen, L.-J., Wang, S., Hesse, M., Ergun, R. E., Moore, T., Giles, B., et al. (2019). Electron diffusion regions in magnetotail reconnection under varying guide fields. *Geophysical Research Letters*, *46*, 6230–6238. https://doi.org/10.1029/2019GL082393

Daughton, W. (1999). The unstable eigenmodes of a neutral sheet. *Physics of Plasmas*, *6*(4), 1329–1343. https://doi.org/10.1063/1.873374

Daughton, W. (2003). Electromagnetic properties of the lower-hybrid drift instability in a thin current sheet. *Physics of Plasmas*, *10*(8), 3103–3119. https://doi.org/10.1063/1.1594724

Daughton, W., Scudder, J., & Karimabadi, H. (2006). Fully kinetic simulations of undriven magnetic reconnection with open boundary conditions. *Physics of Plasmas*, *13*(7), 72101. https://doi.org/10.1063/1.2218817

Davidson, R. C., & Gladd, N. T. (1975). Anomalous transport properties associated with the lower-hybrid-drift instability. *The Physics of Fluids*, *18*(10), 1327–1335. https://doi.org/10.1063/1.861021

Davidson, R. C., Gladd, N. T., Wu, C. S., & Huba, J. D. (1977). Effects of finite plasma beta on the lower-hybrid-drift instability. *The Physics of Fluids*, *20*(2), 301–310. https://doi.org/10.1063/1.861867

Divin, A., Khotyaintsev, Y. V., Vaivads, A., André, M., Markidis, S., & Lapenta, G. (2015). Evolution of the lower hybrid drift instability at reconnection jet front. *Journal of Geophysical Research: Space Physics*, *120*, 2675–2690. https://doi.org/10.1002/2014JA020503

Dungey, J. W. (1953). LXXVI. conditions for the occurrence of electrical discharges in astrophysical systems. *Philosophical Magazine Series 7*, *44*(354), 725–738. https://doi.org/10.1080/14786440708521050

Gladd, N. T. (1976). The lower hybrid drift instability and the modified two stream instability in high density theta pinch environments. *Plasma Physics*, *18*(1), 27–40. https://doi.org/10.1088/0032-1028/18/1/002

Hirose, A., & Alexeff, I. (1972). Electrostatic instabilities driven by currents perpendicular to an external magnetic field. *Nuclear Fusion*, *12*(3), 315.

Huba, J. D., & Wu, C. S. (1976). Effects of a magnetic field gradient on the lower hydrid drift instability. *The Physics of Fluids*, *19*(7), 988–994. https://doi.org/10.1063/1.861594

Ji, H., Terry, S., Yamada, M., Kulsrud, R., Kuritsyn, A., & Ren, Y. (2004). Electromagnetic fluctuations during fast reconnection in a laboratory plasma. *Physical Review Letters*, *92*, 115001. https://doi.org/10.1103/PhysRevLett.92.115001

Krall, N. A., & Liewer, P. C. (1971). Low-frequency instabilities in magnetic pulses. *Physical Review A*, *4*, 2094–2103. https://doi.org/10.1103/PhysRevA.4.2094

Lapenta, G., Brackbill, J. U., & Daughton, W. S. (2003). The unexpected role of the lower hybrid drift instability in magnetic reconnection in three dimensions. *Physics of Plasmas*, *10*(5), 1577–1587. https://doi.org/10.1063/1.1560615

Lapenta, G., Pucci, F., Olshevsky, V., Servidio, S., Sorriso-Valvo, L., Newman, D. L., & Goldman, M. V. (2018). Nonlinear waves and instabilities leading to secondary reconnection in reconnection outflows. *Journal of Plasma Physics*, *84*(1), 715840103. https://doi.org/10.1017/S002237781800003X

Le, A., Daughton, W., Chen, L.-J., & Egedal, J. (2017). Enhanced electron mixing and heating in 3-D asymmetric reconnection at the Earth's magnetopause. *Geophysical Research Letters*, *44*, 2096–2104. https://doi.org/10.1002/2017GL072522

Le, A., Egedal, J., Ohia, O., Daughton, W., Karimabadi, H., & Lukin, V. S. (2013). Regimes of the electron diffusion region in magnetic reconnection. *Physical Review Letters*, *110*, 135004. https://doi.org/10.1103/PhysRevLett.110.135004

Le, A., Stanier, A., Daughton, W., Ng, J., Egedal, J., Nystrom, W. D., & Bird, R. (2019). Three-dimensional stability of current sheets supported by electron pressure anisotropy. *Physics of Plasmas*, *26*(10), 102114. https://doi.org/10.1063/1.5125014

Nakamura, T. K. M., Umeda, T., Nakamura, R., Fu, H. S., & Oka, M. (2019). Disturbance of the front region of magnetic reconnection outflow jets due to the Lower-Hybrid drift instability. *Physical Review Letters*, *123*, 235101. https://doi.org/10.1103/PhysRevLett.123.235101

Ng, J., Chen, L.-J., Le, A., Stanier, A., Wang, S., & Bessho, N. (2020). Dataset for lower-hybrid-drift vortices in the electron-scale magnetic reconnection layer. https://doi.org/10.5281/zenodo.3928914

Phan, T. D., Kistler, L. M., Klecker, B., Haerendel, G., Paschmann, G., Sonnerup, B. U. O., et al. (2000). Extended magnetic reconnection at the Earth's magnetopause from detection of bi-directional jets. *Nature*, *404*(6780), 848–850.

Price, L., Swisdak, M., Drake, J. F., Cassak, P. A., Dahlin, J. T., & Ergun, R. E. (2016). The effects of turbulence on three-dimensional magnetic reconnection at the magnetopause. *Geophysical Research Letters*, *43*, 6020–6027. https://doi.org/10.1002/2016GL069578

Roytershteyn, V., Daughton, W., Karimabadi, H., & Mozer, F. S. (2012). Influence of the lower-hybrid drift instability on magnetic reconnection in asymmetric configurations. *Physical Review Letters*, *108*, 185001. https://doi.org/10.1103/PhysRevLett.108.185001

Vasyliunas, V. M. (1975). Theoretical models of magnetic field line merging. *Reviews of Geophysics*, *13*(1), 303–336.

von Goeler, S., Stodiek, W., & Sauthoff, N. (1974). Studies of internal disruptions and $m = 1$ oscillations in tokamak discharges with soft X-ray techniques. *Physical Review Letters*, *33*(20), 1201–1203. https://doi.org/10.1103/PhysRevLett.33.1201

Yamada, M., Kulsrud, R., & Ji, H. (2010). Magnetic reconnection. *Reviews of Modern Physics*, *82*, 603–664. https://doi.org/10.1103/RevModPhys.82.603